Biomaterials 161 (2018) 228–239

Contents lists available at ScienceDirect

Biomaterials

journal homepage: www.elsevier.com/locate/biomaterials

Lysosomal deposition of copper oxide nanoparticles triggers HUVEC cells death

Jun Zhang [1], Zhen Zou [1], Bin Wang, Ge Xu, Qiong Wu, Yuchan Zhang, Zhiyi Yuan, Xi Yang, Chao Yu*

Institute of Life Sciences, Chongqing Medical University, Chongqing, 400016, PR China

ARTICLE INFO

Article history:
Received 10 July 2017
Received in revised form
20 January 2018
Accepted 27 January 2018
Available online 3 February 2018

Keywords:
CuONPs
Vascular endothelial cell
Lysosomal deposition
Cu ions
Autophagy
Cytotoxicity

ABSTRACTS

The increasing use of copper oxide nanoparticles (CuONPs) has led to major concerns regarding both the predominant physicochemical properties and the potential toxic effects on the environment and human health. The objective of this study is to explore the possible mechanisms underlying the toxicity of CuONPs in vascular endothelial cells. We found that CuONPs induced the cell death in human umbilical vein endothelial cells (HUVECs) through a caspase-independent pathway. Our results also demonstrated that CuONPs were prevalently deposited within lysosomes. The lysosomal deposition of CuONPs led to lysosomal dysfunction, resulting in the impairment of autophagic flux and the accumulation of undegraded autophagosomes. Nevertheless, blockage of the lysosomal deposition of CuONPs could significantly attenuate HUVEC cell death. Interestingly, we found that the inhibition of lysosomal deposition of CuONPs reduced the release of Cu ions, which has been considered as the crucial factor for the toxicity of CuONPs. In summary, our results indicate that the lysosomal deposition of CuONPs (along with the enhanced release of Cu ions form CuONPs) triggers CuONPs-induced HUVEC cell death. Our findings provide an insight into the mechanism of toxicity to the cardiovascular system induced by toxic metal oxide nanoparticles exposure.

1. Introduction

Copper oxide nanoparticles (CuONPs) exhibit unique optical, mechanical, electrical and catalytic properties; they are widely used in the fields of industry, life sciences, and healthcare [1]. For instance, they have been extensively used as oxidation catalysts [2,3], electric conductors [4,5], magnetic storage media [6], energy storage material [7], and antimicrobials reagent against *Escherichia coli*, *Staphylococcus aureus* and *Bacillus subtilis* [8,9]. However, with the increased application of CuONPs, concerns have been raised regarding its potential toxicity to environmental and human health [10–15].

Nanoparticles invade the organism primarily through lung inhalation routes [16]. Its continuous exposure can induce dose-dependent lung inflammation and cellular damage [17]. Also, the inhaled nanoparticles have an especially significant influence on the cardiovascular system [18]. The precise pathway, through which nanoparticles affect the cardiovascular process, has not yet been defined, although two hypotheses have been proposed. The indirect pathway is that inhaled particles provoke an inflammatory response in the lungs, with consequent release of prothrombotic and inflammatory cytokines into the circulation [19–21]. Another proposed pathway is that inhaled nanoparticles can penetrate the air-blood barrier into the systemic circulation, subsequently accumulate at sites of vascular inflammation and directly influence the cardiovascular functions [22,23].

Previous *in vitro* studies confirmed that CuONPs induce high toxicity to human lung epithelial cells A549, liver hepatocellular carcinoma cells HepG2, leukemic cells HL60, bronchial epithelial cells and human breast cancer cells MCF7 [24–28]. The toxicity of CuONPs mainly originates from both the CuO particles and the released Cu ions [29,30]. CuONPs can directly trigger oxidative stress and inflammation [31], resulting in significant genotoxicity and cytotoxicity [24,29,32]. However, the molecular mechanisms underlying the toxicity of CuONPs and the toxic effects of CuONPs to cells in the cardiovascular system have not been described.

Recently, lysosomal dysfunctions have been considered as a

* Corresponding author. Institute of Life Sciences, Chongqing Medical University, No.1 Yixueyuan Road, Yuzhong District, Chongqing 400016, PR China.
E-mail address: yuchaom@163.com (C. Yu).
[1] Authors contributed equally to this work.

https://doi.org/10.1016/j.biomaterials.2018.01.048
0142-9612/

possible mechanism of nanoparticles-induced toxicity. Lysosomes play an essential role in the degradation of both dysfunctional proteins and damaged organelles to maintain cellular homeostasis [33]. Lysosomal dysfunction could induce lysosomal membrane permeabilization (LMP), which is a recognized cell death mechanism resulting from the release of cathepsins and other hydrolases from the lysosomal lumen to the cytosol [34,35]. Increasing evidence indicates that the cellular deposition of nanoparticles can cause autophagic stress and lysosomal dysfunctions, thus lead to the toxicological consequences [36,37]. But the specific roles of lysosome in CuONPs-induced cytotoxicity, particularly in the vascular endothelium, have not been clarified.

Vascular endothelium could be directly exposed to toxic nanoparticles in the bloodstream, suggesting the potential pathogenic relevance between nanoparticles and vascular endothelium. The objective of this study is to explore the possible mechanisms of CuONPs toxicity in vascular endothelial cells. We investigated the adverse effects of CuONPs on HUVECs and discussed the contributions of both the Cu ions released from CuONPs and lysosomal deposition in CuONPs-triggered HUVEC cell death. The findings will help to better understand the toxic effects of nanoparticles exposure to the cardiovascular system.

2. Materials and methods

2.1. Nanoparticles and characterization

CuONPs (<50 nm particle size, #544868) were purchased from Sigma Aldrich (St. Louis, MO, USA). According to the manufacturer's illustration, the size of the CuONPs was less than 50 nm size. Further characterization was carried out to determine different physicochemical characteristics of CuONPs. The size and morphology of the CuONPs were observed using transmission electron microscopy (TEM, JEM-1400Plus). Chemical composition was analyzed by energy dispersive X-ray spectroscopy (EDS) using a JEOL JSM6700F microscope (Japan). The hydrodynamic diameter and an estimation of surface charge of CuONPs were determined by dynamic light scattering (DLS) using a Malvern Zetasizer Nano ZEN3600 (Malvern, Massachusetts, USA).

2.2. Reagents

Tetramethylrhodamine ethyl ester perchlorate (TMRE, #87917), ammonium tetrathiomolybdate (TTM, #323446) and 3-methyladenine (3-MA, #M9281) were purchased from Sigma Aldrich (St. Louis, MO, USA). Annexin V-FITC apoptosis analysis kit was purchased from Sungene Biotech (Tianjin, China). Z-VAD-fmk (#C1202) and penicillin-streptomycin (#C0222) were purchased from Beyotime (Jiangsu, China). Staurosporine (#9953) were purchased from Cell Signaling Technology (Danvers, MA, USA). Wortmannin (#S2758) was purchased from Selleck Chemicals (Houston, TX, USA). Ammonium chloride (NH_4Cl, #A116373) was purchased from Aladdin Chemistry (Shanghai, China). Bafilomycin A1 (Baf A1, #sc-201550) was purchased from Santa Cruz Biotechnology (Santa Cruz, CA, USA). LysoTracker Green DND-26 (#L7526) and Dulbecco's Modified Eagle's Medium (DMEM, #11965-092) was purchased from Thermo Fisher Scientific (Waltham, MA, USA). Fetal bovine serum (FBS, #04-001-1ACS) was purchased from Biological Industries (Kibbutz Beit Haemek, Israel).

2.3. Cell culture and treatment

The HUVEC cell line was purchased from the American Type Culture Collection (Rockville, MD, USA) and was cultured in DMEM medium supplemented with 10% FBS and 100 U penicillin-streptomycin at 37 °C with 5% CO_2. We constructed the specific HUVEC cells, which stably expressing the mRFP-GFP-LC3 (tfLC3) fusion protein. HUVEC-tfLC3 cells were isolated by inoculation of mRFP-GFP-LC3 lentivirus followed by selection with puromycin. For transfection with pEGFP-LC3 plasmid (a gift from Tamotsu Yoshimori) [38], cells were seeded in 12-well plates overnight and then transfected with plasmid using Lipofectamine 2000 (Invitrogen, CA, USA) for 24 h according to the manufacturer's instructions. For treatment with CuONPs, cells were seeded in 12-well plates for overnight and then treated with CuONPs, which were suspended in culture medium and vigorously vortexed for several seconds before exposure. Finally, cells were harvested and assays were conducted. For pretreatment with chemical inhibitors, cells were pretreated with Z-VAD-fmk, NH_4Cl, Baf A1, or TTM for 1 h, hereafter were treated with CuONPs in the culture medium.

2.4. Cell viability assays

Cell viability was determined by MTS assay (#G5430, Promega, Madison, WI, USA) as previously described [39]. Briefly, HUVEC cells were seeded into 96-well plates and cultured overnight. After treatment for the indicated time points shown in figure captions, MTS/PMS solution in culture medium was added to each well of the plate and the plate was incubated at 37 °C for 1 h. The absorbance of each well was measured at 490 nm using a VERS Amax Microplate Reader (Molecular Devices Corp, Sunnyvale, CA, USA).

2.5. Flow cytometry assays

Flow cytometry assays were performed as previously described [40]. An annexin V-FITC apoptosis analysis kit was used for apoptotic cells detection. Tetramethylrhodamine ethyl ester perchlorate (TMRE) (5 nM) was used to measure mitochondrial membrane potential. LysoTracker Green DND-26 (50 nM) was used to probe functional acidic lysosomes. All flow cytometry assays were performed on a BD Influx Cell Sorter (BD Biosciences, San Jose, CA, USA), and results were analyzed using BD FACS software. All assays were conducted in triplicate at least three times.

2.6. Transmission electron microscopy

The morphologies of CuONPs were characterized by transmission electron microscopy (TEM). Briefly, a few drops of CuONPs aqueous solution were added on carbon-coated copper grids, dried at room temperature, and detected by TEM (Hitachi-7500, Japan). For cell morphology assay by TEM, cells were centrifuged at 1000 g for 5 min after trypsinization and fixed with 4% glutaraldehyde in 0.2 M of phosphate-buffered saline (PBS, pH 7.4) for 2 h at 4 °C, washed three times with PBS, and then postfixed with 1% osmium tetroxide in 0.2 M PBS for 1 h at 4 °C. The cell samples were dehydrated in a graded series of alcohol and acetone, and then embedded in Epon 816 (Electron Microscopy Sciences, USA). The ultrathin sections were obtained by using a Leica ultramicrotome (Leica Microsystems, Buffalo Grove, IL, USA), stained with uranyl acetate and lead citrate, and finally examined under a JEM-1400Plus transmission electron microscope (JEOL Ltd. Tokyo, Japan).

2.7. Western blotting assays

For western blotting assays, HUVECs cells were washed three times with cold PBS and lysed in radioimmunoprecipitation assay (RIPA) lysis buffer (Beyotime, Jiangsu, China) supplemented with protease inhibitor cocktail (Roche, Basel, Switzerland). After lysis on ice for 30 min, cell lysates were centrifuged for 30 min at 4 °C at

12,000 g. The supernatants were subjected to SDS-PAGE and proteins were transferred onto polyvinylidene fluoride (PVDF) membrane (Merck Millipore, Billerica, MA, USA). The membranes were incubated with corresponding primary and secondary antibodies. The protein signals were detected using a New-SUPER ECL Substrate Kit (Keygen Biotech, Nanjing, China). The following antibodies were used in this study: a Cleaved Caspase Antibody Sampler Kit (1:1000, Cell Signaling Technology, #9929), LC3 (1:1000, Cell Signaling Technology, #12741), Beclin-1 (1:1000, Cell Signaling Technology, #3495), Atg5 (1:1000, Cell Signaling Technology, #12994), SQSTM1/p62 (1:1000, Cell Signaling Technology, ab109012), lysosomal-associated membrane protein 1 (LAMP-1, 1:1000, Cell Signaling Technology, #9091), LAMP-2 (1:500, Santa Cruz Biotechnology, sc-18822) and β-actin (1:3000, Bioss, bs-0061R).

2.8. Immunofluorescence staining

Cells seeded on coverslips were washed three times with precold PBS, fixed with 4% paraformaldehyde (PFA) in PBS for 15 min at room temperature and subsequently permeabilized with 0.2% Triton X-100 in PBS for 10 min at room temperature. Cells were incubated with blocking solution (2% BSA and 22.52 mg/ml glycine in PBS) for 1 h at room temperature, and then incubated with primary antibodies diluted in blocking solution overnight. After at least 3 washes in PBS, cells were incubated with secondary antibodies and 4′,6-diamidino-2-phenylindole (DAPI, Molecular Probes, Eugene, OR, USA) diluted in blocking solution for 1 h. Cells were then washed three times with PBS and the coverslips were sealed with nail polish. Fluorescence was examined using confocal laser scanning microscopy (Nikon, Tokyo, Japan), and the images were analyzed using NIS-Elements Viewer 4.20. The following antibodies were used in this study: LAMP-1 (1:200, Cell Signaling Technology, #9091), LAMP-2 (1:100, Santa Cruz Biotechnology, sc-18822), Alexa Fluor 594-conjugated donkey anti-rabbit immunoglobulin G (IgG, 1:500, Molecular Probes, A-21207) and Alexa Fluor 488-conjugated donkey anti-mouse IgG (1:500, Molecular Probes, A-21202).

2.9. RNA interference

All small interfering RNAs (siRNAs) were purchased from GenePharma (Shanghai, China). Cells were mock-transfected or transfected with siRNAs using Lipofectamine RNAiMAX (#13778150, Invitrogen) for 48 h according to the manufacturer's instructions and knockdown efficiencies of the siRNAs were determined by western blotting analysis. The siRNA sequences used in this study are as follows:

siBeclin-1: 5′-GCUGCCGUUAUACUGUUCUtt-3′,
si-LAMP-1: 5′-CAAUGCGAGCUCCAAAGAAtt-3′,
si-LAMP-2: 5′-GCGGUCUUAUGCAUUGGAAtt-3′,
Negative control siRNA: 5''-UUCUCCGAACGUGUCACGUtt-3'.

2.10. Copper ions assays

Cu ions released in cell culture medium were assayed with a QuantiChrom Copper Assay Kit (BioAssay Systems, Hayward, CA, USA) as described previously [24,41]. Briefly, after 24 h of treatment with CuONPs, culture medium supernatant was collected and 35 μl of Reagent A was mixed by vortexing with 100 μl of each sample. One hundred 50 μL of working solution (mixing 5 μl Reagent B and 150 μl Reagent C) were transferred to each sample and incubated for 5 min at room temperature. The amount of Cu ions in the medium was assayed by measuring the absorbance at 359 nm under a

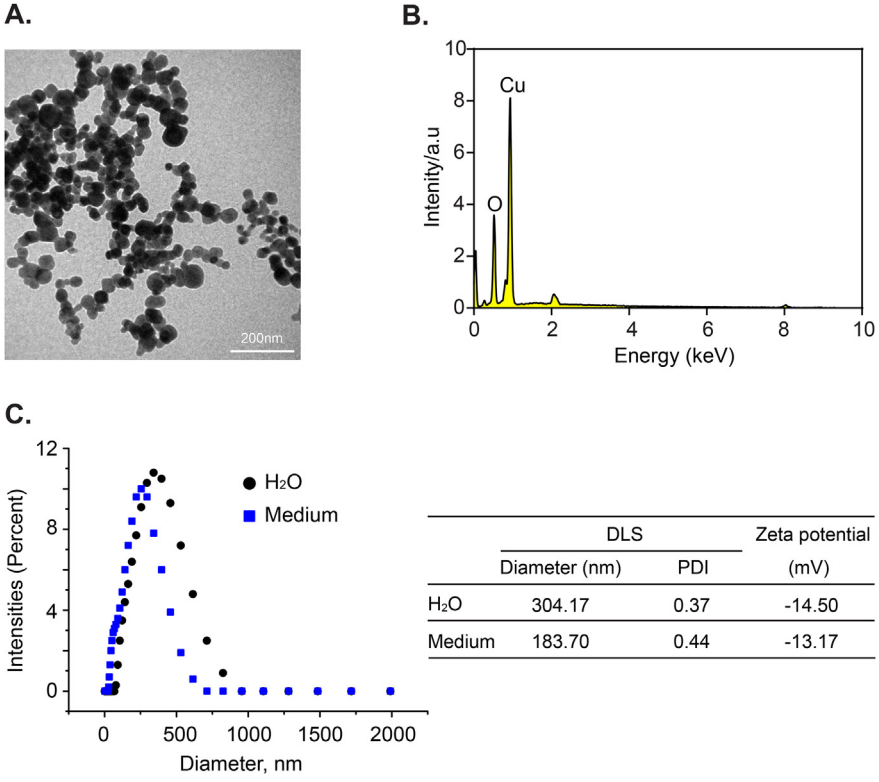

	DLS		Zeta potential
	Diameter (nm)	PDI	(mV)
H_2O	304.17	0.37	-14.50
Medium	183.70	0.44	-13.17

Fig. 1. Physical characteristics of CuONPs. **(A)** A representative TEM image of CuONPs. **(B)** The EDS spectrum of CuONPs. **(C)** The hydrodynamic diameters and zeta-potentials of CuONPs were measured by dynamic light scattering (DLS) using a Malvern Zetasizer Nano-ZS instrument.

VERS Amax Microplate Reader (Molecular Devices Corp, Sunnyvale, CA, USA). Results were normalized in comparison with the control and expressed as fold increase.

2.11. Statistical analysis

Data are shown as the mean ± standard deviation (S.D.). Each experiment was repeated at least three times. All statistical tests were conducted using Prism 5.0 (GraphPad Software, San Diego, CA, USA). $^{*}p < 0.05$ indicates statistical significance, $^{**}p < 0.01$ indicates high significance, and NS indicates no significance.

3. Results

3.1. Characterization of copper oxide nanoparticles (CuONPs)

CuONPs were characterized by transmission electron microscopy (TEM), energy dispersive spectroscopy (EDS) and dynamic

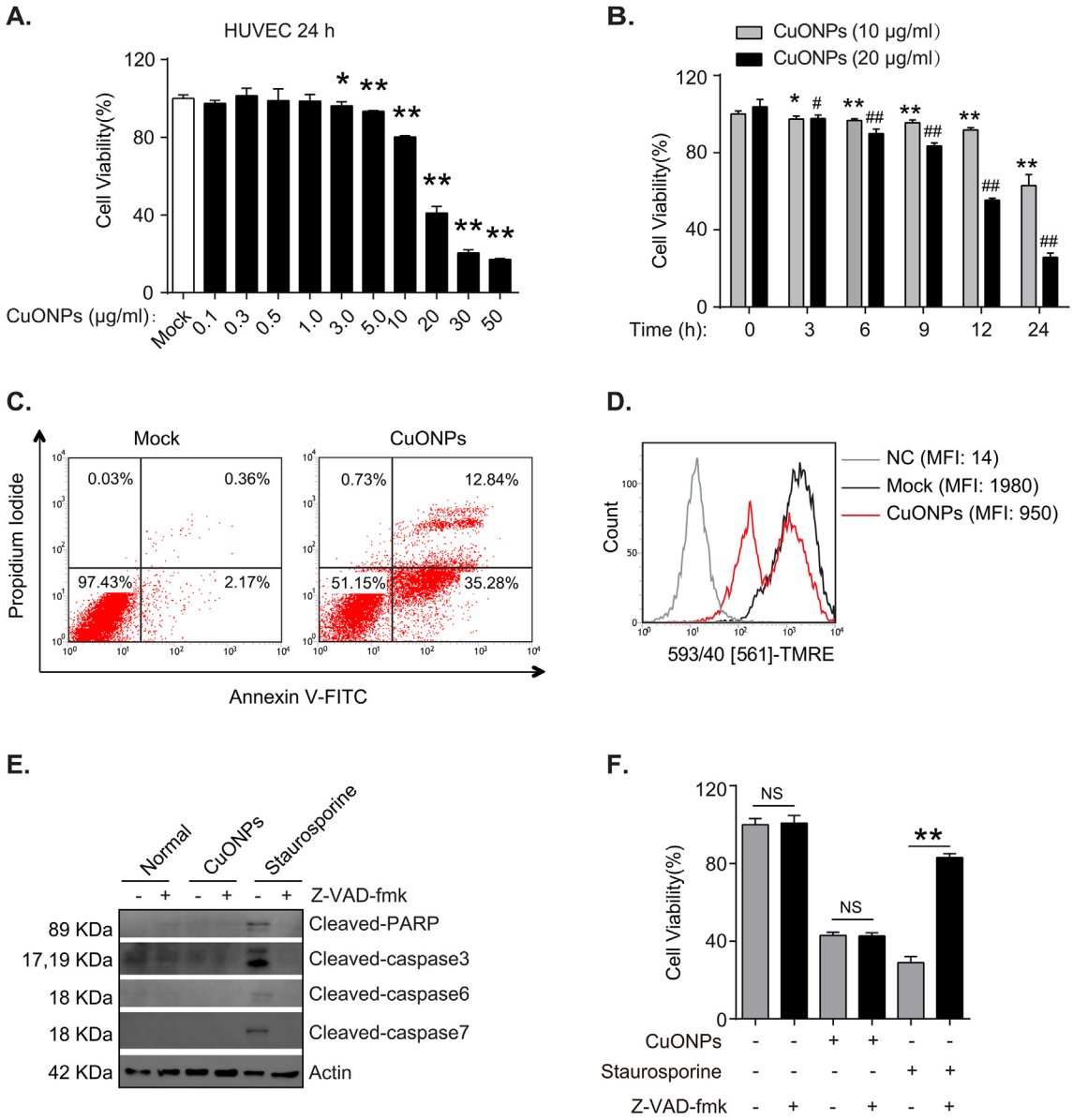

Fig. 2. CuONPs triggered HUVEC apoptotic-like cell death. **(A)** MTS analysis of HUVEC cells treated with various concentrations of CuONPs (0.1, 0.3, 0.5, 1, 3, 5, 10, 20, 30, 50 μg/ml) for 24 h. Data are representative of three independent experiments, and values are expressed in mean ± S.D. One-way ANOVA analysis with Tukey's test was performed for statistical analysis. $^{*}p < 0.05$ and $^{**}p < 0.01$. **(B)** MTS analysis of HUVEC cells exposed to 20 μg/ml of CuONPs for 3, 6, 9, 12, or 24 h. Data are representative of three independent experiments, and values are expressed in mean ± S.D. One-way ANOVA analysis with Tukey's test performed for statistical analysis. $^{*}p < 0.05$ and $^{**}p < 0.01$ versus 10 μg/ml CuONPs treatment for 0 h; $^{\#}p < 0.05$ and $^{\#\#}p < 0.01$ versus 20 μg/ml CuONPs treatment for 0 h. **(C)** Detection of apoptotic cells in CuONPs-treated HUVEC cells using flow cytometry after annexin V-FITC/propidium iodide staining. HUVEC cells were treated with 20 μg/ml of CuONPs for 24 h. The relative percentage of live (lower-left quadrant), early apoptotic (lower-right quadrant), and late apoptotic and necrotic (upper-right quadrant) cells are shown. **(D)** Flow cytometry analysis of HUVEC cells treated with 20 μg/ml of CuONPs for 24 h following staining with TMRE (1 nM). MFI, mean fluorescence intensity. **(E)** Western blotting analysis of cleaved-caspases levels in HUVEC cells treated with CuONPs (20 μg/ml) at indicated time points. Cell extracts from HUVECs treatment with staurosporine (a well-known inducer of apoptosis) were used as a positive apoptosis control. Actin served as the loading control. **(F)** HUVEC cells were pretreated with Z-VAD-fmk (50 μM) for 1 h, followed by treatment of 20 μg/ml of CuONPs or 1 μM of staurosporine for 24 h. Then, cells viability was determined by MTS assay. Data are representative of three independent experiments and values are expressed in mean ± S.D. One-way ANOVA analysis with Tukey's test was performed for statistical analysis ($^{**}p < 0.01$; NS, not significance).

light scattering (DLS), respectively. TEM images showed that CuONPs exhibited different shapes and sizes. Small particles were spherical, whereas larger particles were irregular in shapes. Most particles had an average diameter of 52.5 ± 12.7 nm, which was calculated by randomly measuring the diameter of 250 particles in the representative TEM images (Fig. 1A). To further characterize the CuONPs, EDS was employed for elemental analysis. As shown in Fig. 1B, there are specific peaks that correspond to Cu and O elements in the EDS image. The average of hydrodynamic radius and zeta potential in ultrapure water were 304.17 nm and −14.50 mV, respectively, while the average of hydrodynamic radius and zeta potential in the culture medium were 183.70 nm and −13.17 mV, respectively (Fig. 1C).

3.2. CuONPs exposure induced apoptotic-like cell death in HUVEC

To determine the effects of CuONPs on vascular endothelial cells, the cell viability of HUVECs was examined using MTS assay after

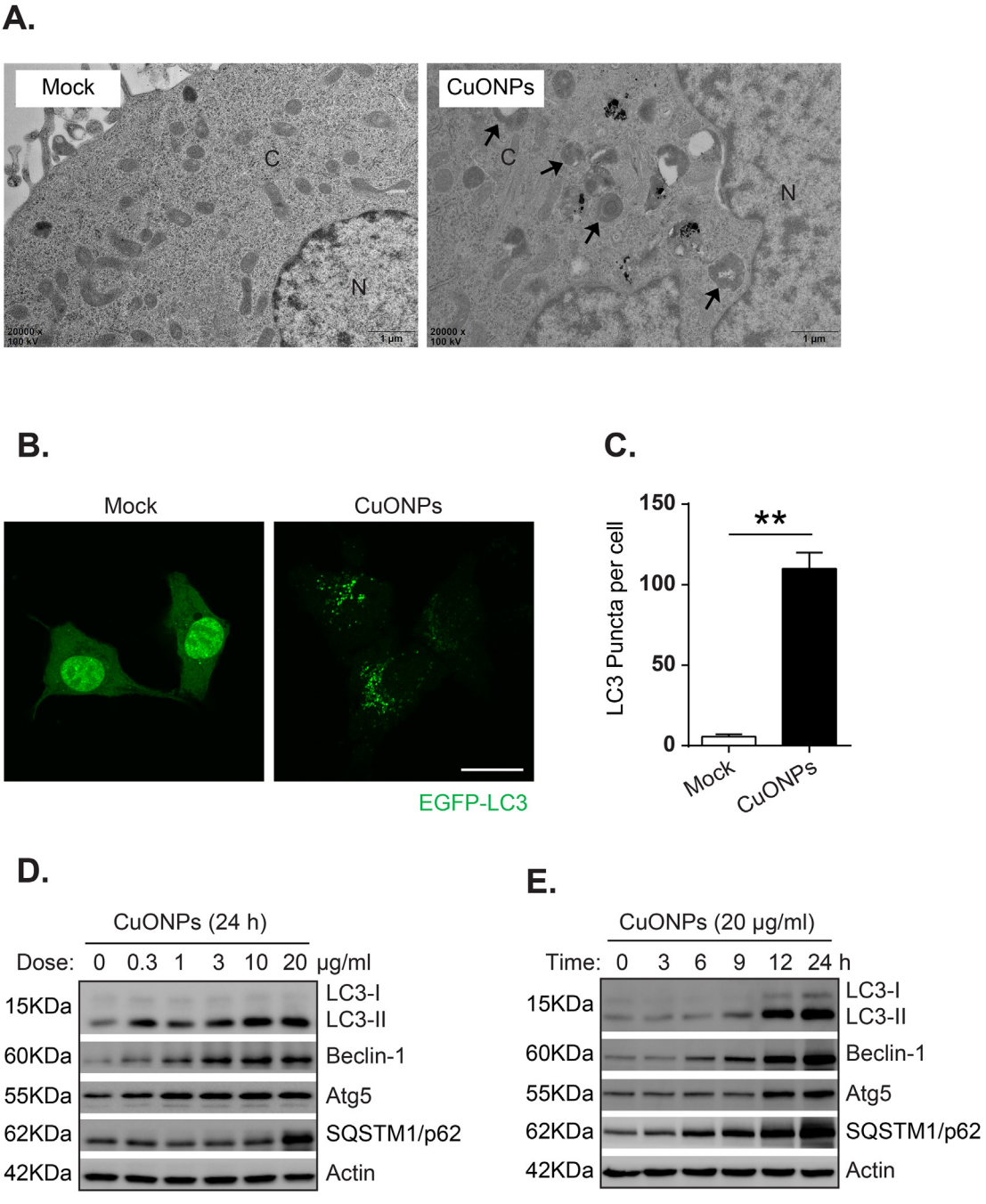

Fig. 3. Autophagosomes accumulation in CuONPs-treated HUVECs. **(A)** TEM images of HUVEC cells exposed to 20 μg/ml CuONPs for 0 or 12 h. Black arrows indicate autophagosomes. Images are the representative of three independent experiments. N, Nucleus; C, Cytoplasm. **(B)** Images of EGFP-LC3 puncta in HUVEC cells, which were transfected with pEGFP-LC3 for 24 h and then treated with 20 μg/ml of CuONPs for 24 h. Scale bar: 50 μm. **(C)** The EGFP-LC3 puncta per cell was quantified using ImageJ software. Data (mean ± SD) are the representative of at least three independent experiments. Unpaired *t*-tests were performed for statistical analysis. $^{**}p < 0.01$. **(D)** Western blotting analysis the levels of autophagy-related proteins in HUVECs treated with various concentrations of CuONPs for 24 h. Images are the representative of three independent experiments. **(E)** Western blotting analysis the levels of autophagy-related proteins in HUVECs treated with 20 μg/ml CuONPs for 3, 6, 9, 12, or 24 h.

exposure to different concentrations of CuONPs (0.1–50 μg/ml) for 24 h or CuONPs (10 and 20 μg/ml, respectively) for various time points. Results showed that CuONPs treatment triggered HUVEC death at a dose of 5–50 μg/ml (Fig. 2A). Meanwhile, a time-dependent effect of CuONPs-induced cell death was observed. The cell death began at 3 h after CuONPs exposure, and the substantial cell death was observed at the 24 h (Fig. 2B). Furthermore, flow cytometry assay after annexin V-FITC/propidium iodide staining showed that CuONPs exposure increased the percentage of cells in both early (Fig. 2C, lower right quadrant) and late apoptosis (Fig. 2C, upper right quadrant). Another hallmark of apoptotic cell death, the collapse of mitochondrial membrane potential, was also observed in CuONPs-treated cells using TMRE staining, which is suitable for quantifying changes in mitochondrial membrane potential in live cells by fluorescent microscopy and flow cytometry (Fig. 2D and Fig. S1). Caspase is a family of cysteine acid proteases, which are central regulators of apoptosis [42]. Hence, we investigated whether CuONPs-induced apoptotic-like death was caspase-dependent. Staurosporine, a protein kinase C inhibitor, was used as a positive apoptosis inducer [43]. As shown in Fig. 2E, no cleaved caspase-3, 6, 7 were detected in CuONPs-treated cells. However, apparent cleavages of poly (ADP-ribose) polymerase (PARP) and caspase-3, 6, 7 were detected in staurosporine-treated HUVECs. And Z-VAD-fmk (a pancaspase inhibitor) could inhibit staurosporine-induced cleavage of PARP and caspase-3, 6, 7. MTS assay results also showed that Z-VAD-fmk failed to rescue CuONPs-induced cell death while naturally reducing staurosporine-induced apoptotic cell death (Fig. 2E). The above results indicate that CuONPs trigger HUVECs apoptotic-like cell death in a caspase-independent manner.

3.3. CuONPs induced autophagosomes accumulation in HUVECs

We investigated whether autophagy is involved in cell death

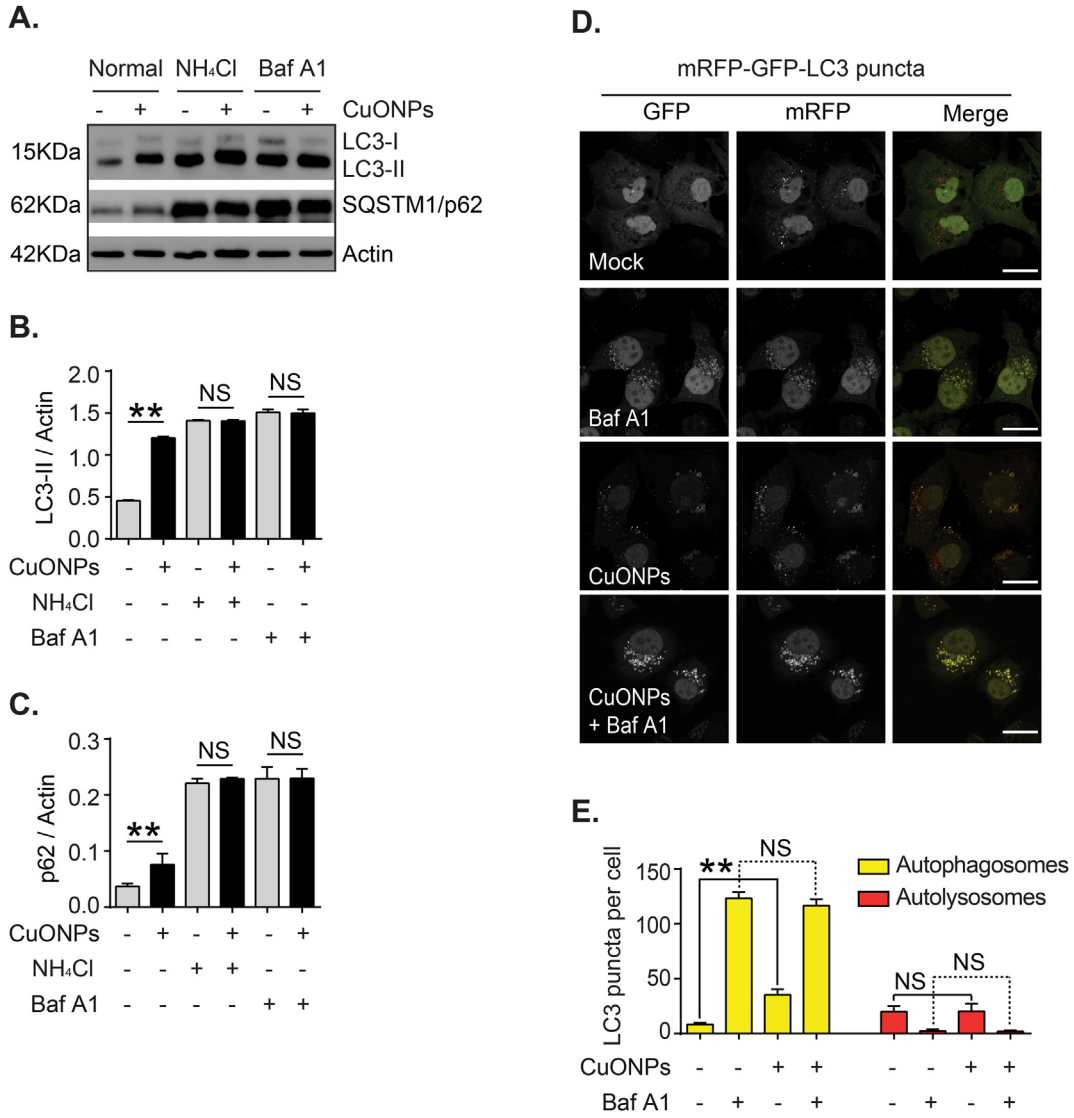

Fig. 4. CuONPs exposure blocked the fusion of autophagosomes with lysosomes. **(A)** Western blotting assays were conducted to characterize the levels of LC3 and SQSTM1/p62 in HUVEC cells pretreated with NH_4Cl (10 mM) and Baf A1 (100 nM) for 1 h before being exposed to 20 μg/ml of CuONPs for 24 h. Actin was used as the loading control. **(B and C)** The intensity of bands was quantified using ImageJ software. The data are the mean ± S.D. of three independent assays. Nonparametric Mann-Whitney tests were performed for statistical analysis (**$p < 0.01$; NS, not significance). **(D)** HUVECs stably expressing of a mRFP-GFP-LC3 fusion gene were treated either with Baf A1 (100 nM), CuONPs (20 μg/ml), or Baf A1 plus CuONPs for 24 h. Confocal images were obtained after 4% PFA fixation for 10 min (Scale bar, 50 μm). Images are representative of three independent experiments. **(E)** The number of yellow puncta (autophagosomes) and the number of red puncta (autolysosomes) were counted using ImageJ software. Data are representative of three independent experiments. One-way ANOVA analysis with Tukey's tests were performed for statistical analysis (**$p < 0.01$; NS, not significance).

induced by CuONPs in HUVECs. TEM images showed that autophagosomes in HUVEC cells increased dramatically at 12 h after treatment with CuONPs (Fig. 3A). The number of LC3 puncta, an ideal marker to monitor autophagosomes, also increased markedly in CuONPs-treated HUVECs cells (Fig. 3B and C). Then, we analyzed the levels of autophagy-related proteins using western blotting assay. Results showed that the levels of LC3-II, Beclin-1 (the mammalian orthologue of yeast Atg6), and Atg5 (an E3 ubiquitin ligase, which is necessary for LC3 lipidation in autophagy) significantly increased after treatment with CuONPs (Fig. 3D and E). These results indicate that CuONPs exposure can induce autophagosomes accumulation in HUVECs. To elucidate the interplay between autophagy and CuONPs-induced cytotoxicity, two phosphatidylinositol-4,5-bisphosphate 3-kinase (PI3K) inhibitors (3-MA or wortmannin) was applied to inhibit autophagy. The MTS assay results showed that the inhibition of autophagy did not obviously alleviate HUVECs cell death induced by CuONPs (Fig. S2A). Similar results were obtained using siRNA-mediated knockdown of the key autophagy-related gene Beclin-1 (Fig. S2B and C). These results suggest that autophagy does not directly contribute to CuONPs-induced HUVECs death. Interestingly, there was a similar increase of SQSTM1/p62 (a multifunctional adapter in autophagy) in CuONPs-treated cells (Fig. 3D and E).

3.4. CuONPs induced the accumulation of autophagosomes by blocking autophagic flux

It is well known that the simultaneous increase of SQSTM1/p62 and LC3-II may indicate cellular autophagic flux impairment [44]. We measured the autophagic flux in CuONPs-treated cells. With the treatment of either NH_4Cl or Baf A1 (the inhibitors of autophagosome-lysosome fusion), there were no differences in either LC3-II or SQSTM1/p62 levels compared with the normal control group (Fig. 4A–C), indicating that the autophagic flux in HUVEC cells was blocked after CuONPs exposure. To test the hypothesis that the accumulation of autophagosomes might results from the lack of lysosomal degradation, we constructed the specific HUVECs expressing the mRFP-GFP-LC3 fusion protein. Tandem fluorescent-tagged LC3 (mRFP-EGFP-LC3) is constructed through fusing green and red fluorescent proteins with LC3, which is used for monitoring autophagic flux based on different pH stability of mRFP and EGFP fluorescent proteins. The acidic environment quenches the EGFP fluorescent signal yet has much less effect on mRFP. Therefore, mRFP-EGFP-LC3 shows a GFP and mRFP fluorescence signals in neutral autophagosome (merged as yellow puncta), but exhibits the mRFP fluorescence signal in acidic autolysosome (red puncta). Comparing with the untreated cells, in the HUVEC-tfLC3 cells treated with CuONPs, the autophagosome puncta (yellow) were markedly increased, but the autolysosome puncta (red)

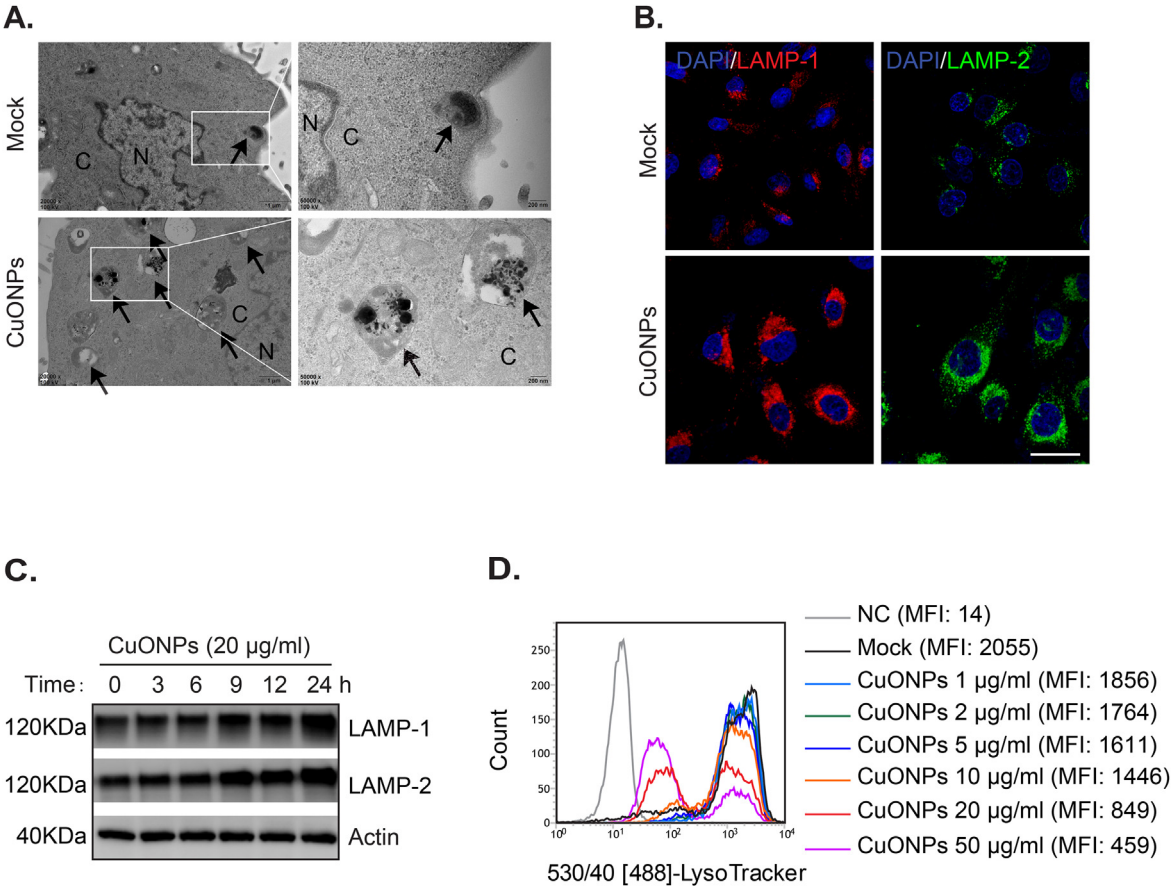

Fig. 5. CuONPs accumulation within lysosomes causeed lysosome impairment. **(A)** TEM images of HUVEC cells untreated (Mock) or treated with 20 μg/ml CuONPs for 24 h. N, Nucleus; C, Cytoplasm. Black arrows indicate lysosomes. **(B)** Confocal microscopy assay of the LAMP-1 and LAMP-2 after immunofluorescence staining in mock cells or cells treated with 20 μg/ml of CuONPs for 24 h. Scale bar: 50 μm. **(C)** Western blotting analysis LAMP-1 and LAMP-2 expression in HUVECs treated with 20 μg/ml of CuONPs for 0, 3, 6, 9, 12, or 24 h. Images are representative of three independent experiments. **(D)** HUVEC cells were exposed to various concentrations of CuONPs for 24 h. Flow cytometry assay was then used to detect the LysoTracker fluorescence signals. NC, HUVECs unstained with LysoTracker. Mock, HUVECs without treatment with CuONPs. MFI: Mean fluorescence intensity.

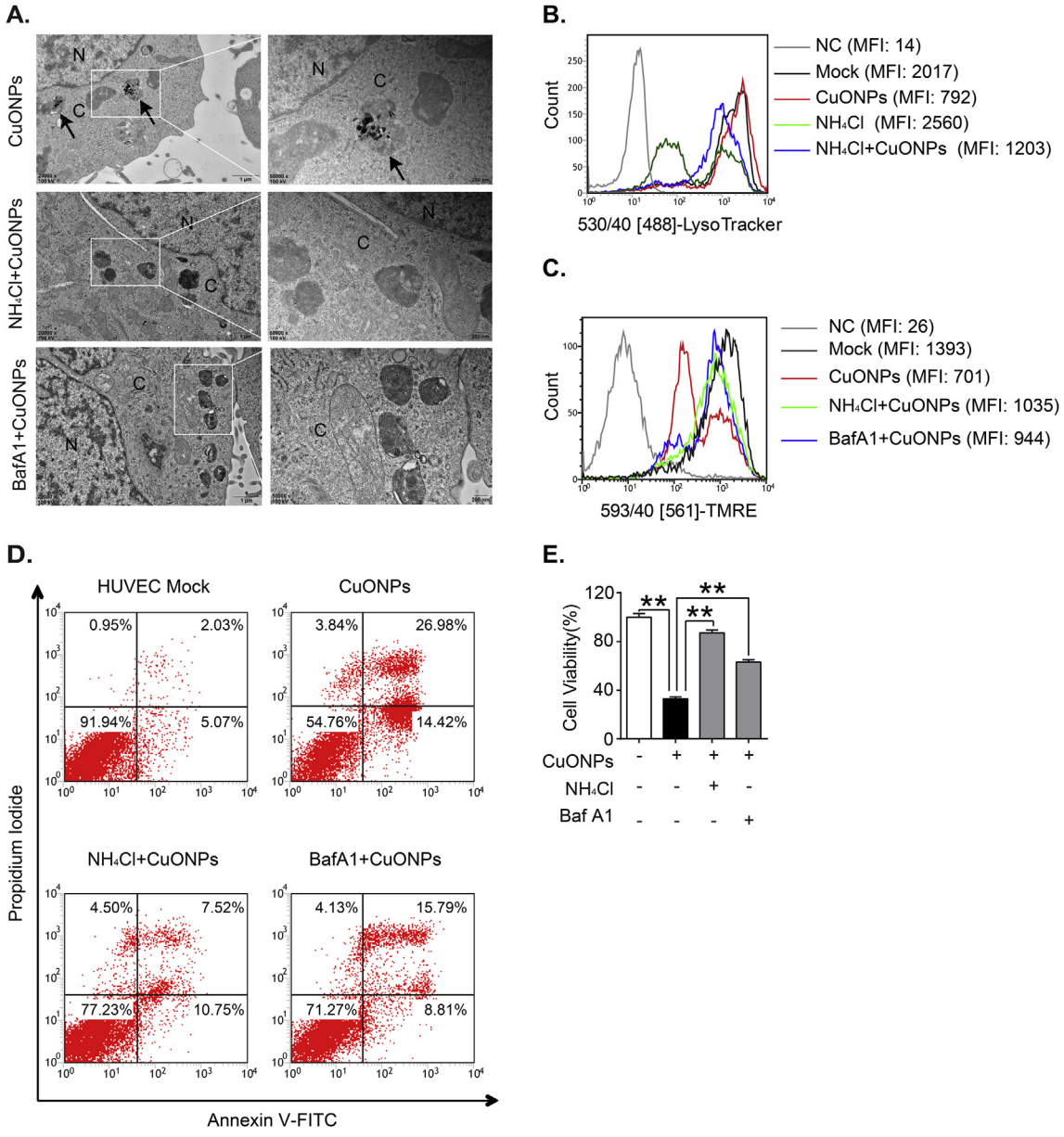

Fig. 6. Blocking lysosomal deposition of CuONPs reduced HUVEC cell death. **(A)** HUVEC cells were pretreated with NH_4Cl (10 mM) or Baf A1 (100 nM) for 1 h and then was treated with 20 μg/ml of CuONPs for 24 h. Cells were collected and TEM assay was conducted. N, Nucleus; C, Cytoplasm; Black arrows indicate CuONPs in lysosomes. **(B)** Flow cytometry assay HUVEC cells treated with 20 μg/ml of CuONPs for 24 h following staining with LysoTracker probe (50 nM). NC, HUVECs unstained with LysoTracker. Mock, HUVECs without treatment with CuONPs. MFI: Mean fluorescence intensity. **(C)** Flow cytometry assay HUVEC cells treated with 20 μg/ml of CuONPs for 24 h following staining with TMRE (1 nM). NC, HUVECs unstained with TMRE. Mock, HUVECs without treatment with CuONPs. MFI: Mean TMRE fluorescence intensity. **(D)** Apoptotic cells were detected using flow cytometry after annexin V-FITC/propidium iodide staining. Lower-left quadrant, live cells; lower-right quadrant, early apoptotic cells; upper-right quadrant, late apoptotic and necrotic cells. **(E)** HUVEC cells were pretreated with NH_4Cl (10 mM) or Baf A1 (100 nM) followed by 20 μg/ml CuONPs treatment. MTS analysis was performed to detect the cell viability at 24 h after treatment. Data are representative of three independent experiments. One-way ANOVA analysis with Tukey's tests were performed for statistical analysis ($^{**}p < 0.01$).

were no significant difference (Fig. 4D and E). We proposed that the CuONPs-induced accumulation of autophagosomes in HUVECs is possibly attributed to the impairment of autophagosome-lysosome fusion.

3.5. CuONPs lysosomal deposition impaired lysosomal function

It is accepted that lysosomes are the crucial death signal integrator in response to various stimuli [45]. To investigate whether lysosomes are involved in CuONPs-induced cell death, we examined the biological effects of CuONPs on HUVEC lysosomes. From TEM images, we found that CuONPs accumulated in lysosomes and triggered lysosomes enlargement and aberrant accumulation (Fig. 5A). The high-level accumulation of CuONPs within lysosomes may perturb lysosomal function. Lysosome-associated membrane protein-1 and 2 (LAMP-1 and LAMP-2) are the two most abundant lysosomal membrane proteins, which are widely used as lysosome markers [46]. Immunofluorescence staining displayed that LAMP-1 and LAMP-2 aggregated at the perinuclear area in CuONPs-treated cells, while evenly distributed in the cytoplasm of untreated cells (Fig. 5B). Western blotting also showed that the levels of LAMP-1 and LAMP-2 increased, suggesting an aberrant accumulation of

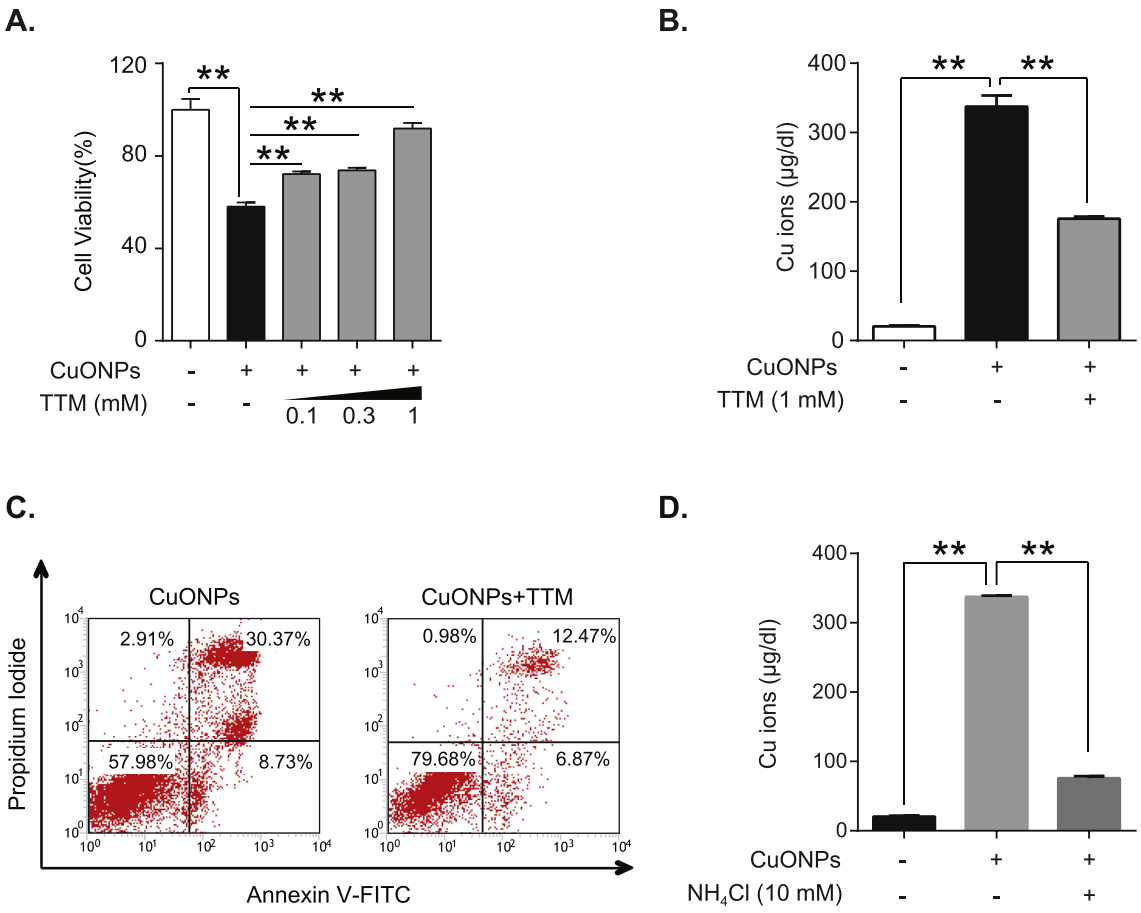

Fig. 7. The release of Cu ions from CuONPs induced lysosomal dysfunction and HUVEC cell death. **(A)** HUVEC cells were pretreated with different concentrations of Cu ions chelator TTM and subsequently treated with 20 μg/ml of CuONPs for 24 h. MTS analysis was performed to detect the cell viability. Data are representative of three independent experiments (**$p < 0.01$). **(B)** HUVEC cells were pretreated with Cu ions chelator TTM (1 mM) and then treated with 20 μg/ml of CuONPs for 24 h. The released Cu ions in culture medium was assayed with QuantiChrom Copper Assay Kit. Mock, HUVEC cells without treatment with CuONPs. Data (mean ± SD) are representative of at least three independent experiments. Unpaired *t*-tests were performed for statistical analysis. **$p < 0.01$. **(C)** Flow cytometry assay was used to determine apoptotic cells after annexin V-FITC/propidium iodide staining. Lower-left quadrant, live cells; lower-right quadrant, early apoptotic cells; upper-right quadrant, late apoptotic and necrotic cells. **(D)**. HUVEC cells were pretreated with NH_4Cl (10 mM) and treated with 20 μg/ml of CuONPs for 24 h. The released Cu ions in culture medium was assayed with a QuantiChrom Copper Assay Kit. Data (mean ± SD) are representative of at least three independent experiments. Unpaired *t*-tests were performed for statistical analysis. **$p < 0.01$.

lysosomes in HUVECs by CuONPs treatment (Fig. 5C). The LysoTracker is a fluorescent acidotropic probe for labeling and tracking functional acidic lysosomes in live cells [47]. Flow cytometry assay showed that the LysoTracker fluorescent signal was severely decreased after CuONPs treatment, indicating lysosomal impairment in CuONPs-treated cells (Fig. 5D). Collectively, these data suggest that CuONPs deposited within lysosomes and impaired the functions of lysosomes.

3.6. Blocking lysosomal deposition of CuONPs attenuated apoptotic cell death

To further explore whether lysosomal deposition is indeed related to CuONPs-induced cell death, we pretreated HUVECs with NH_4Cl or Baf A1 before CuONPs exposure. NH_4Cl is a lysosomotropic reagent which can neutralize the lysosomal pH. Baf A1 (a specific inhibitor of the H^+-ATPase) can also cause an increment of lysosomal pH. Thus, NH_4Cl or Baf A1 treatment can block autophagosomes-lysosome fusion. As shown in Fig. 6A, NH_4Cl or Baf A1 pretreatment almost entirely blocked the lysosomal deposition of CuONPs. Flow cytometry assay also displayed that there was a stronger LysoTracker fluorescence signal in NH_4Cl-pretreated HUVECs compared with NH_4Cl non-pretreated cells, suggesting that NH_4Cl pretreatment relieved the impairment of lysosomes in CuONPs-treated HUVECs (Fig. 6B). TMRE staining revealed that NH_4Cl or Baf A1 pretreatment inhibited the mitochondrial transmembrane potential collapse induced by CuONPs (Fig. 6D and Fig. S3). We also observed that NH_4Cl or Baf A1 pretreatment could drastically reduce apoptotic cell death (Fig. 6C) and significantly rescued the HUVEC cells viability compared with a non-pretreatment group (Fig. 6E). In addition, we investigated the effects of NH_4Cl treatment on the response of CuONPs-induced inflammatory in endothelial cells and showed that NH_4Cl treatment obviously inhibited CuONPs-induced upregulation of tumor necrosis factor (TNF)-α, intercellular adhesion molecule 1 (ICAM1) and interleukin (IL-6) (Fig. S4). Subsequently, we knocked down LAMP-1 and LAMP-2 expression to further investigate lysosomal deposition in CuONPs-induced cell death. Knockdown efficiency was examined by western blotting assay (Fig. S5A). Flow cytometry assay displayed that LAMP-1 or LAMP-2 knockdown (especially LAMP-2) obviously reduce apoptotic cell death induced by CuONPs (Fig. S5B). Cell viability assay further confirmed that LAMP-1/2 knockdown could obviously alleviate CuONPs-induced HUVECs cell death (Fig. S5C). These data indicate that blocking lysosomal deposition of CuONPs attenuated apoptotic cell death.

3.7. CuONPs toxicity on HUVECs resulted from the released Cu ions

It has been reported that CuONPs could be dissolved and release toxic Cu ions into the surrounding media. Thus, we investigated whether the toxic effects of CuONPs on the lysosomal dysfunction and apoptotic cell death of HUVECs derives from the released Cu ions. HUVEC cells were pretreated with Cu ions chelator ammonium tetrathiomolybdate (TTM) before CuONPs treatment. MTS assay showed that TTM pretreatment significantly attenuated CuONPs-induced HUVEC cell death (Fig. 7A). Then, we examined the released Cu ions in the culture medium after CuONPs treatment. Results showed that CuONPs obviously induced the release of Cu ions into HUVEC cell culture medium (Fig. 7B). Flow cytometry assay showed the Cu ions chelator pretreatment significantly reduced the apoptotic-like cells induced by CuONPs compared with non-pretreatment group (Fig. 7C). Moreover, we found that NH_4Cl pretreatment decreased intracellular Cu ions concentration, indicating that the lysosomal deposition of CuONPs might facilitate the release of Cu ions from CuONPs-treated (Fig. 7D).

4. Discussion

Recent studies have provided rare insights into the interaction between the toxicity of metal oxide nanoparticles and the cardiovascular system [48–50]. However, the underlying mechanisms of nanoparticles exposure to cardiovascular injury have not been fully elucidated. In this study, we found that CuONPs exposure induced apoptotic-like cell death in HUVEC vascular endothelial cells, based on membrane blebbing (annexin V-FITC/propidium iodide staining) and mitochondrial dysfunction (TMRE staining) after CuONPs treatment (Fig. 2C and D). However, several classical apoptotic substrates (caspase-3/6/7 and PARP) were not altered in CuONPs-treated HUVEC cells (Fig. 2E). Therefore, we inferred that a caspase-independent cell death pathway might be involved in CuONPs-induced cytotoxicity.

Autophagic cell death is one of the caspase independent cell deaths [51], which is defined as cell death by autophagic stress and morphologically characterized by large-scale autophagosomes in the cytoplasm but in the absence of chromatin condensation [52]. Sun et al. [25] demonstrated that CuONPs exposure could induce significant autophagic cell death in A549, while the inhibition of autophagy by 3-MA decreased CuONPs-induced cell death. In the current study, we found that CuONPs markedly induced the accumulation of autophagic vacuoles (Fig. 3), but the inhibition of autophagy with pharmacological autophagy inhibitor (3-MA or wortmannin) or Beclin-1 knockdown failed to ameliorate CuONPs-induced HUVEC death (Fig. S3). Our results indicated that CuONPs-induced HUVEC death is along with autophagy, not caused by autophagy stress (autophagic cell deaths). Certainly, the caspase-independent cell death is an extremely comprehensive concept; it may include autophagic cell death, caspase-independent apoptosis, necrosis, pyroptosis, ferroptosis, necroptosis, oncosis, necoroptosis and so on. It could be an arduous challenge to illustrate the specific form of CuONPs-induced cell death. We expect to address this question in our ongoing study.

Autophagosomes accumulation indicates either autophagy induction or impairment of autophagic flux [53]. Therefore, we further explored the possible mechanism underlying the accumulation of autophagosomes in CuONPs-treated HUVECs. Results showed that the accumulation of autophagosomes in CuONPs-treated HUVECs resulted from the impairment of autophagic flux, rather than autophagy activation (Fig. 4). Generally, the impairment of autophagic flux may indicate lysosomal dysfunction [44]. Our results revealed that CuONPs prominently deposited within lysosomes of HUVEC cells after 24 h after exposure (Fig. 5A). This finding is consistent with previous studies showing that the lysosomes are the most common intracellular sites of nanoparticles sequestration and degradation [54,55]. Upon cellular exposure, CuONPs may initially enter HUVEC cells via endocytic pathways. The endocytosed CuONPs can then be transported to lysosomes. In addition, we also observed that the lysosomal deposition of CuONPs induced abnormal enlargement and aggregation of lysosomes (Fig. 5). Lysosomes are mainly involved in receiving and degrading phagocytosed macromolecules [56]. We hypothesized that the massive deposition of CuONPs in lysosomes might severely damage lysosomal degradation capacity. We also confirmed that the blockage of the lysosomal deposition of CuONPs in HUVECs, through regulating lysosomal pH and LAMP-1/2 knockdown, respectively, attenuates CuONPs-induced HUVECs death (Fig. 6 and Fig. S4). These results indicated that lysosomes play an important role in CuONPs-induced HUVECs cell death. In this respect, lysosomal deposition may be a novel mechanism of CuONPs toxicity in HUVEC.

The plausible mechanisms through which CuONPs lysosomal deposition triggers HUVEC death is also be explored in the present study. Our results showed that Cu ions are released from CuONPs-treated cells, while treatment with a Cu ions chelator could decrease intracellular Cu ions concentration and significantly reduce CuONPs-induced cell death, indicating that the release of Cu ions from CuONPs directly triggers HUVEC death (Fig. 7). Cu is one of the indispensable elements for maintaining homeostasis and cause toxicity through inducing oxidative stress and DNA damage when it exceed the physiological tolerance range [57]. This finding is consistent with previously published reports that Cu ions released from CuONPs are related to A549 cells genome expression in response to CuONPs exposure [29]. Recently, we revealed that the release of zinc ions from zinc oxide nanoparticles (ZnONPs) in acidic lysosomes directly trigger cell death in A549 lung epithelial cells [58]. In this study, we revealed that blocking lysosomal deposition of CuONPs could decrease intracellular Cu ions concentration indicating that CuONPs may release more Cu ions after deposition within lysosomes because of lysosomal acidic conditions.

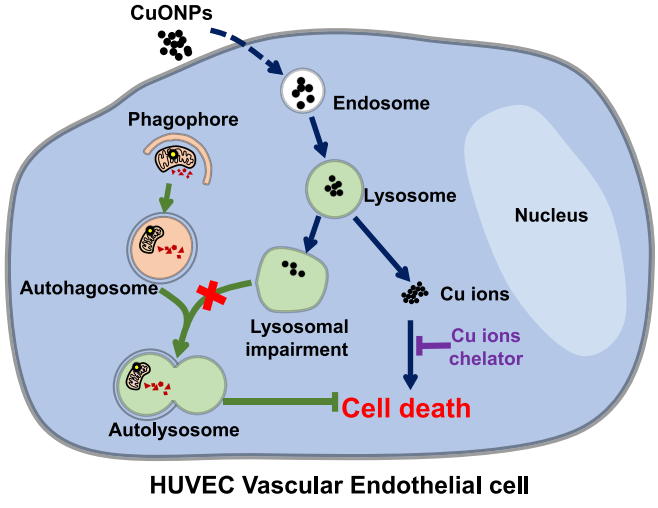

Fig. 8. The schematic of the mechanism of CuONPs-induced HUVEC cell death. CuONPs may initially enter HUVEC cells via endocytic pathway and then be transported to the lysosome. The lysosomal deposition of CuONPs causes the lysosome dysfunction and results in both the autophagic flux impairment and the accumulation autophagosomes, consequently triggers HUVEC cell death. Meanwhile, the lysosomal deposition of CuONPs promotes the release of Cu ions, which also exacerbates the CuONPs-induced HUVEC cell death.

In summary, we found that CuONPs could be deposited within the lysosomes of HUVECs and released abundant Cu ions. The lysosomal deposition of CuONPs caused lysosome impairment, which results in both the blockage of autophagic flux and the accumulation of undegraded autophagosomes, and consequently triggered HUVEC cell death. Also, the lysosomal deposition of CuONPs promoted the release of Cu ions from CuONPs, which in turn exacerbated the CuONPs-induced cells death in HUVEC (Fig. 8). Our study shed new light on the mechanism underlying the toxicity induced by metal oxide nanoparticles in the cardiovascular system.

Acknowledgements

We thank Ziguo Luo, Xiaogang Liao, Jingchuan Fan and Aijia Song for their help with the transmission electron microscopy, and Xiaoyun Dou for her help with confocal microscopy. We are grateful to the Professor Yu's lab members Yazhen Niu, Jun Chen, Zhiyong Tang and Yan Li for their help with nanoparticles characterizations. We thank Ronald D. Frost for his help improving our revised manuscript. This work was supported in part by the National Natural Science Foundation of China (81500343 and 81370403) and the Chongqing Research Program of Basic Research and Frontier Technology (cstc2015jcyjA10002, cstc2015jcyjBX0053 and cstc2017jcyjAX0162).

Appendix A. Supplementary data

Supplementary data related to this article can be found at https://doi.org/10.1016/j.biomaterials.2018.01.048.

Declaration of interest

The authors declare no conflict of interest.

Authors' contributions

Jun Zhang and Zhen Zou conceived and designed this project. Jun Zhang, Zhen Zou, Qiong Wu, Yuchan Zhang, Zhiyi Yuan and Xi Yang carried out all cell biological and biochemical experiments. Bin Wang contributed to the confocal microscope experiment. Ge Xu contributed to electron microscopy. Jun Zhang and Zhen Zou analyzed the data. Jun Zhang, Zhen Zou and Chao Yu wrote the manuscript with inputs and revision from all authors.

References

[1] M. Suleiman, M. Mousa, A. Hussein, B. Hammouti, T.B. Hadda, I. Warad, Copper (II)-oxide nanostructures: synthesis, characterizations and their applications–review, J. Mater. Environ. Sci. 4 (2013) 792–797.
[2] F. Diao, F. Tian, W. Liang, H. Feng, Y. Wang, Mechanistical investigation on the self-enhanced photocatalytic activity of CuO/Cu2O hybrid nanostructures by density functional theory calculations, Phys. Chem. Chem. Phys. 18 (2016) 27967–27975.
[3] K. Brown, M. Tegoni, M. Prudencio, A.S. Pereira, S. Besson, J.J. Moura, et al., A novel type of catalytic copper cluster in nitrous oxide reductase,, Nat. Struct. Biol. 7 (2000) 191–195.
[4] K.J. Choi, H.W. Jang, One-dimensional oxide nanostructures as gas-sensing materials: review and issues, Sensors 10 (2010) 4083–4099.
[5] A.A. Abdel-Khalek, S.R. Badran, M.A. Marie, Toxicity evaluation of copper oxide bulk and nanoparticles in Nile tilapia, Oreochromis niloticus, using hematological, bioaccumulation and histological biomarkers, Fish Physiol. Biochem. 42 (2016) 1225–1236.
[6] I. Singh, K. Landfester, A. Chandra, R. Munoz-Espi, A new approach for crystallization of copper(II) oxide hollow nanostructures with superior catalytic and magnetic response,, Nanoscale 7 (2015) 19250–19258.
[7] A.S. Arico, P. Bruce, B. Scrosati, J.M. Tarascon, W. van Schalkwijk, Nanostructured materials for advanced energy conversion and storage devices, Nat. Mater. 4 (2005) 366–377.
[8] G. Ren, D. Hu, E.W. Cheng, M.A. Vargas-Reus, P. Reip, R.P. Allaker, Characterisation of copper oxide nanoparticles for antimicrobial applications, Int. J. Antimicrob. Agents 33 (2009) 587–590.
[9] A. Azam, A.S. Ahmed, M. Oves, M.S. Khan, A. Memic, Size-dependent antimicrobial properties of CuO nanoparticles against Gram-positive and -negative bacterial strains, Int. J. Nanomed. 7 (2012) 3527–3535.
[10] J.M. Pettibone, A. Adamcakova-Dodd, P.S. Thorne, P.T. O'Shaughnessy, J.A. Weydert, V.H. Grassian, Inflammatory response of mice following inhalation exposure to iron and copper nanoparticles, Nanotoxicology 2 (2008) 189–204.
[11] Z. Wang, N. Li, J. Zhao, J.C. White, P. Qu, B. Xing, CuO nanoparticle interaction with human epithelial cells: cellular uptake, location, export, and genotoxicity, Chem. Res. Toxicol. 25 (2012) 1512–1521.
[12] M. Alaraby, A. Hernandez, R. Marcos, New insights in the acute toxic/genotoxic effects of CuO nanoparticles in the in vivo Drosophila model, Nanotoxicology 10 (2016) 749–760.
[13] M.S. Boyles, C. Ranninger, R. Reischl, M. Rurik, R. Tessadri, O. Kohlbacher, et al., Copper oxide nanoparticle toxicity profiling using untargeted metabolomics, Part. Fibre Toxicol. 13 (2016) 49.
[14] G. Bhabra, A. Sood, B. Fisher, L. Cartwright, M. Saunders, W.H. Evans, et al., Nanoparticles can cause DNA damage across a cellular barrier, Nat. Nanotechnol. 4 (2009) 876–883.
[15] B. Nowack, T.D. Bucheli, Occurrence, behavior and effects of nanoparticles in the environment, Environ. Pollut. 150 (2007) 5–22.
[16] W. Yang, J.I. Peters, R.O. Williams 3rd, Inhaled nanoparticles–a current review, Int. J. Pharm. 356 (2008) 239–247.
[17] I. Gosens, F.R. Cassee, M. Zanella, L. Manodori, A. Brunelli, A.L. Costa, et al., Organ burden and pulmonary toxicity of nano-sized copper (II) oxide particles after short-term inhalation exposure, Nanotoxicology 10 (2016) 1084–1095.
[18] H.S. Choi, Y. Ashitate, J.H. Lee, S.H. Kim, A. Matsui, N. Insin, et al., Rapid translocation of nanoparticles from the lung airspaces to the body, Nat. Biotechnol. 28 (2010) 1300–1303.
[19] T.D. Nelin, A.M. Joseph, M.W. Gorr, L.E. Wold, Direct and indirect effects of particulate matter on the cardiovascular system, Toxicol. Lett. 208 (2012) 293–299.
[20] J.W. Park, I.C. Lee, N.R. Shin, C.M. Jeon, O.K. Kwon, J.W. Ko, et al., Copper oxide nanoparticles aggravate airway inflammation and mucus production in asthmatic mice via MAPK signaling, Nanotoxicology 10 (2016) 445–452.
[21] S.T. Larsen, P. Jackson, S.S. Poulsen, M. Levin, K.A. Jensen, H. Wallin, et al., Airway irritation, inflammation, and toxicity in mice following inhalation of metal oxide nanoparticles, Nanotoxicology 10 (2016) 1254–1262.
[22] M.R. Miller, J.B. Raftis, J.P. Langrish, S.G. McLean, P. Samutrtai, S.P. Connell, et al., Inhaled nanoparticles accumulate at sites of vascular disease, ACS Nano 11 (2017) 4542–4552.
[23] L.E. Yu, L.-Y. Lanry Yung, C.-N. Ong, Y.-L. Tan, K. Suresh Balasubramaniam, D. Hartono, et al., Translocation and effects of gold nanoparticles after inhalation exposure in rats, Nanotoxicology 1 (2007) 235–242.
[24] J.P. Piret, D. Jacques, J.N. Audinot, J. Mejia, E. Boilan, F. Noel, et al., Copper(II) oxide nanoparticles penetrate into HepG2 cells, exert cytotoxicity via oxidative stress and induce pro-inflammatory response, Nanoscale 4 (2012) 7168–7184.
[25] T. Sun, Y. Yan, Y. Zhao, F. Guo, C. Jiang, Copper oxide nanoparticles induce autophagic cell death in A549 cells, PLoS One 7 (2012) e43442.
[26] D. Laha, A. Pramanik, J. Maity, A. Mukherjee, P. Pramanik, A. Laskar, et al., Interplay between autophagy and apoptosis mediated by copper oxide nanoparticles in human breast cancer cells MCF7, Biochim. Biophys. Acta 1840 (2014) 1–9.
[27] Y. Rodhe, S. Skoglund, I. Odnevall Wallinder, Z. Potacova, L. Moller, Copper-based nanoparticles induce high toxicity in leukemic HL60 cells, Toxicol. Vitro 29 (2015) 1711–1719.
[28] A. Thit, H. Selck, H.F. Bjerregaard, Toxic mechanisms of copper oxide nanoparticles in epithelial kidney cells, Toxicol. Vitro 29 (2015) 1053–1059.
[29] N. Hanagata, F. Zhuang, S. Connolly, J. Li, N. Ogawa, M. Xu, Molecular responses of human lung epithelial cells to the toxicity of copper oxide nanoparticles inferred from whole genome expression analysis, ACS Nano 5 (2011) 9326–9338.
[30] D. Wang, Z. Lin, T. Wang, Z. Yao, M. Qin, S. Zheng, et al., Where does the toxicity of metal oxide nanoparticles come from: the nanoparticles, the ions, or a combination of both? J. Hazard Mater. 308 (2016) 328–334.
[31] C. Angele-Martinez, K.V. Nguyen, F.S. Ameer, J.N. Anker, J.L. Brumaghim, Reactive oxygen species generation by copper(II) oxide nanoparticles determined by DNA damage assays and EPR spectroscopy, Nanotoxicology 11 (2017) 278–288.
[32] M. Shi, H.S. Kwon, Z. Peng, A. Elder, H. Yang, Effects of surface chemistry on the generation of reactive oxygen species by copper nanoparticles, ACS Nano 6 (2012) 2157–2164.
[33] P. Boya, F. Reggiori, P. Codogno, Emerging regulation and functions of autophagy, Nat. Cell Biol. 15 (2013) 713–720.
[34] S.T. Stern, P.P. Adiseshaiah, R.M. Crist, Autophagy and lysosomal dysfunction as emerging mechanisms of nanomaterial toxicity, Part. Fibre Toxicol. 9 (2012) 20.
[35] P. Boya, G. Kroemer, Lysosomal membrane permeabilization in cell death, Oncogene 27 (2008) 6434–6451.
[36] I. Schutz, T. Lopez-Hernandez, Q. Gao, D. Puchkov, S. Jabs, D. Nordmeyer, et al., Lysosomal dysfunction caused by cellular accumulation of silica nanoparticles, J. Biol. Chem. 291 (2016) 14170–14184.
[37] X. Ma, Y. Wu, S. Jin, Y. Tian, X. Zhang, Y. Zhao, et al., Gold nanoparticles induce

autophagosome accumulation through size-dependent nanoparticle uptake and lysosome impairment, ACS Nano 5 (2011) 8629–8639.
[38] Y. Kabeya, N. Mizushima, T. Ueno, A. Yamamoto, T. Kirisako, T. Noda, et al., LC3, a mammalian homologue of yeast Apg8p, is localized in autophagosome membranes after processing, EMBO J. 19 (2000) 5720–5728.
[39] B. Wang, J. Zhang, C. Chen, G. Xu, X. Qin, Y. Hong, et al., The size of zinc oxide nanoparticles controls its toxicity through impairing autophagic flux in A549 lung epithelial cells, Toxicol. Lett. 285 (2017) 51–59.
[40] X. Qin, J. Zhang, B. Wang, G. Xu, Z. Zou, LAMP-2 mediates oxidative stress-dependent cell death in Zn^{2+}-treated lung epithelium cells, Biochem. Biophys. Res. Commun. 488 (2017) 177–181.
[41] J.P. Piret, S. Vankoningsloo, J. Mejia, F. Noel, E. Boilan, F. Lambinon, et al., Differential toxicity of copper (II) oxide nanoparticles of similar hydrodynamic diameter on human differentiated intestinal Caco-2 cell monolayers is correlated in part to copper release and shape, Nanotoxicology 6 (2012) 789–803.
[42] G. Nunez, M.A. Benedict, Y. Hu, N. Inohara, Caspases: the proteases of the apoptotic pathway, Oncogene 17 (1998) 3237–3245.
[43] T. Tamaoki, H. Nomoto, I. Takahashi, Y. Kato, M. Morimoto, F. Tomita, Staurosporine, a potent inhibitor of phospholipid/Ca++dependent protein kinase, BBRC (Biochem. Biophys. Res. Commun.) 135 (1986) 397–402.
[44] D.J. Klionsky, K. Abdelmohsen, A. Abe, M.J. Abedin, H. Abeliovich, A. Acevedo Arozena, et al., Guidelines for the use and interpretation of assays for monitoring autophagy, Autophagy 12 (2016) 1–222 (3rd edition).
[45] M.E. Guicciardi, M. Leist, G.J. Gores, Lysosomes in cell death, Oncogene 23 (2004) 2881–2890.
[46] K.K. Huynh, E.L. Eskelinen, C.C. Scott, A. Malevanets, P. Saftig, S. Grinstein, LAMP proteins are required for fusion of lysosomes with phagosomes, EMBO J. 26 (2007) 313–324.
[47] B. Chazotte, Labeling lysosomes in live cells with LysoTracker, Cold Spring Harb. Protoc. 2011 (2011) pdb prot5571.
[48] J. Duan, Y. Yu, Y. Li, Z. Sun, Cardiovascular toxicity evaluation of silica nanoparticles in endothelial cells and zebrafish model, Biomaterials 34 (2013) 5853–5862.
[49] K. Donaldson, R. Duffin, J.P. Langrish, M.R. Miller, N.L. Mills, C.A. Poland, et al., Nanoparticles and the cardiovascular system: a critical review, Nanomedicine 8 (2013) 403–423.
[50] A. Gojova, B. Guo, R.S. Kota, J.C. Rutledge, I.M. Kennedy, A.I. Barakat, Induction of inflammation in vascular endothelial cells by metal oxide nanoparticles: effect of particle composition, Environ. Health Perspect. 115 (2007) 403–409.
[51] G. Kroemer, S.J. Martin, Caspase-independent cell death, Nat. Med. 11 (2005) 725–730.
[52] G. Kroemer, B. Levine, Autophagic cell death: the story of a misnomer, Nat. Rev. Mol. Cell Biol. 9 (2008) 1004–1010.
[53] N. Mizushima, T. Yoshimori, B. Levine, Methods in mammalian autophagy research, Cell 140 (2010) 313–326.
[54] J. Wang, Y. Yu, K. Lu, M. Yang, Y. Li, X. Zhou, et al., Silica nanoparticles induce autophagy dysfunction via lysosomal impairment and inhibition of autophagosome degradation in hepatocytes, Int. J. Nanomed. 12 (2017) 809–825.
[55] L.Y. Chou, K. Ming, W.C. Chan, Strategies for the intracellular delivery of nanoparticles, Chem. Soc. Rev. 40 (2011) 233–245.
[56] A. Ciechanover, Proteolysis: from the lysosome to ubiquitin and the proteasome, Nat. Rev. Mol. Cell Biol. 6 (2005) 79–87.
[57] C. Gunawan, W.Y. Teoh, C.P. Marquis, R. Amal, Cytotoxic origin of copper(II) oxide nanoparticles: comparative studies with micron-sized particles, leachate, and metal salts, ACS Nano 5 (2011) 7214–7225.
[58] J. Zhang, X. Qin, B. Wang, G. Xu, Z. Qin, J. Wang, et al., Zinc oxide nanoparticles harness autophagy to induce cell death in lung epithelial cells, Cell Death Dis. 8 (2017) e2954.